




Article

# CFD Analysis of Biofouling Effect on Submarine Resistance and Wake

I Ketut Aria Pria Utama <sup>1</sup>, Fertisio Farhan <sup>1</sup>, Ahmad Nasirudin <sup>1</sup>, Rizky Chandra Ariesta <sup>1</sup>  
and Martin Robert Renilson <sup>2,\*</sup>

<sup>1</sup> Department of Naval Architecture, Institut Teknologi Sepuluh Nopember, Surabaya 60111, Indonesia; kutama@na.its.ac.id (I.K.A.P.U.); farhanfertisio@gmail.com (F.F.); anasirudin@na.its.ac.id (A.N.); chandra@its.ac.id (R.C.A.)

<sup>2</sup> Australian Maritime College (AMC), The University of Tasmania, Launceston, TAS 7250, Australia

\* Correspondence: m.renilson@utas.edu.au; Tel.: +61-456-098-900

**Abstract:** It is well known that biofouling increases a ship's resistance and nominal wake. For submarines, any change to the circumferential variation of the nominal wake in the propeller plane will affect the variation of the flow over the propeller blade, and hence the fluctuating forces, and noise, generated by the propeller. The *ANSYS FLUENT* commercial Reynolds-Averaged Navier Stokes Computational Fluid Dynamics solver was used to investigate the influence of both the longitudinal and vertical distribution of biofouling on the resistance and wake, including the circumferential variation of the nominal wake, on a submarine, using the well-known Suboff standard submarine. For the present work, the *k-ε* turbulence model was selected, as this is commonly used in this field and is generally considered acceptable. To handle different boundary layer thicknesses in the flow fields, the whole *y+* formulation was employed, enabling automatic switching between low and high Reynolds boundary wall models. The numerical solver used for the simulations is based on the finite volume method, which discretizes the RANS equations. In this approach, a segregated model was utilized in the solver, and the convection terms were discretized using the second-order upwind scheme to enhance solution accuracy. The criteria for the near wall are between 30 and 100, and the value of *y+* for the present case is 84. It is shown that fouling over only the forward third of the submarine results in a greater increase in resistance than fouling over only the aft third. Fouling over only the lower half of the submarine results in greater resistance than fouling over only the forward third, but less than fouling over the whole of the hull. Fouling over only the forward third of the hull has less influence on the circumferential variation of the wake than fouling over the aft third only of the hull. The results show the importance of keeping the forward area of the hull clean when considering resistance only, whereas keeping the aft area of the hull clean is important when considering the uniformity of the nominal wake into the propeller.

**Keywords:** biofouling; submarine resistance; turbulence; wake; distortion coefficient



**Citation:** Utama, I.K.A.P.; Farhan, F.; Nasirudin, A.; Ariesta, R.C.; Renilson, M.R. CFD Analysis of Biofouling Effect on Submarine Resistance and Wake. *J. Mar. Sci. Eng.* **2023**, *11*, 1312. <https://doi.org/10.3390/jmse11071312>

Academic Editor: Maria Isabel Lamas Galdo

Received: 30 May 2023

Revised: 23 June 2023

Accepted: 23 June 2023

Published: 28 June 2023



**Copyright:** © 2023 by the authors. Licensee MDPI, Basel, Switzerland. This article is an open access article distributed under the terms and conditions of the Creative Commons Attribution (CC BY) license (<https://creativecommons.org/licenses/by/4.0/>).

## 1. Introduction

Marine biofouling generates roughness caused by the accumulation of marine biota such as (bacteria, algae, etc.) carried by currents. Biofouling causes roughness on the submerged surface of the hull, which will affect a ship's frictional resistance and wake. This is a serious problem in the shipping industry as it increases fuel consumption due to increased skin friction on the hull. Ship maintenance costs also increase due to biofouling [1–5]. In extreme cases, roughness due to biofouling can increase the effective power required to maintain the same speed by over 70% [5].

Biofouling will also reduce sonar efficiency and increase self-noise, therefore reducing antisubmarine warfare effectiveness [4]. It has also been pointed out [6,7] that biofouling has the consequence of increasing greenhouse gas emissions. Biofouling is a significant

financial burden to shipping companies through increased fuel consumption and associated maintenance costs; however, the application of antifouling coatings harms marine life. Thus, methods to better understand how to optimize the use of antifouling coatings and dry-docking costs have been developed [7]. In addition, a technique for estimating the effect of biofouling on shaft power using onboard sensors has been developed [8].

Biofouling is a gradual process, with increased fouling occurring over time. One traditional way of allowing for increased fouling over time was developed by the British Admiralty, which assumed an increased frictional allowance of  $\frac{1}{4}$  percent per day in temperate waters and  $\frac{1}{2}$  percent per day in tropical waters [1]. Uzun et al. [9] developed a time-dependent biofouling growth model and used equivalent roughness functions for different surface conditions. Uzun et al. [10] looked at the pattern of barnacle settlement and how this influenced ship resistance and power. They found that the pattern of barnacle settlement caused over 10% difference in frictional resistance and over 20% speed reduction at fixed effective power.

As surface roughness caused by biofouling increases skin friction resistance, its influence on the overall resistance of a marine vehicle will be greater for submarines than for surface ships. This is because the percentage of the total resistance due to skin friction is greater for submarines than for surface ships [11]. This has been investigated recently by Uzun et al. [12,13]. Song et al. [14] also showed that the total resistance coefficient in shallow water increases between 22% and 36% due to biofouling.

Suastika et al. [15] investigated the influence of the longitudinal location of roughness on a flat plate for a number of different configurations and found that with an inhomogeneous roughness, the sequence of the roughness arrangement plays a key role in the resulting overall skin friction coefficient. They found that when the roughness is greatest near the leading edge of the plate, the overall skin friction is greatest.

Uzun et al. [13] also investigated the influence of the longitudinal position of the roughness on a submerged submarine. They found that when the roughness is located in the forward part of the submarine only, the increase in total resistance is greater than when it is located only further aft. The increase in total resistance caused by fouling on only the forward one-third of the hull was almost half that caused by fouling over the whole hull. On the other hand, when the fouling was only over the aft third, the resistance increase was only approximately one-third of the total resistance increase when the whole hull was covered with fouling. Uzen et al. [13] also found that when the roughness was located further aft, this caused a larger increase in nominal wake than when it was further forward.

In addition to increasing skin friction resistance, biofouling will also influence the nominal wake. The combination of the increased resistance, requiring increased propeller rpm, together with the increased nominal wake, will also cause a change in the propeller advance coefficient for a given speed of the submarine. This will influence the propeller efficiency. Uzun et al. [13] showed that the subsequently increased power required by a fully fouled submarine hull may be over 60%, whereas when the fouling is only on the forward third of the hull, the increase in power required is of the order of only 10%. They showed that the increase in power required when only the center third is fouled is similar to that when only the aft third of the hull is fouled.

Uzun et al. [12] showed the influence of roughness on the axial wake at various locations. Although they showed that the presence of the roughness did change the wake distribution, it was not clear from this work what influence this change would have on the flow into the propeller, and hence the noise it generates.

The circumferential distribution of the variation in axial wake will influence the fluctuation in the force on each propeller blade as it rotates through one rotation. This is due to the angle of attack on the blade changing, and hence changing the load on the propeller blade. It will have a major influence on the noise generated by the propeller, which is of great importance to submarines [11].

Seil and Anderson [16] developed the concept of a Distortion Coefficient to quantitatively determine the influence of the variation in circumferential nominal wake on the flow

into the propulsor, and hence provide insight into the effect of this on the noise generated by the propulsor. To date, the influence of biofouling on the nominal wake of a submarine has not been investigated. Thus, although it is possible to deduce that biofouling will increase the drag of a submarine, there is no information on its influence on the variation of the circumferential nominal wake, and hence, on how this will affect the noise generated by the propeller. Clearly, this is of great importance to the operation of a military submarine.

Based on the above background, the present work was carried out to determine the effect on resistance and nominal wake, including the Distortion Coefficient, of attaching biofouling to the full-scale Defence Advanced Research Projects Agency (DARPA) Suboff submarine. The position and extent of the biofouling were examined, and its influence on the nominal wake, in particular the likely influence on noise generated by the propeller, was investigated.

It is recognized that in an ideal situation, the submarine would be kept clean; however, there are reasons such as cost that might limit the extent of the cleaning. In addition, when in a foreign port, there may be the desire to limit the transfer of invasive species carried on the hull [17].

This paper is arranged as follows: Section 2 is a description of the Computational Fluid Dynamics (CFD) approach adopted, including a discussion of the way that the roughness was handled and the grid independence study. The results are presented in Section 3. First, the influence of biofouling on the resistance is given in Section 3.1. Then the effect of biofouling on turbulence is given in Section 3.2, and finally, the effect of biofouling on the wake, including the circumferential non-uniformity of the wake, as defined by the Distortion Coefficient, is given in Section 3.3. The circumferential non-uniformity will have an impact on the noise generated by the propulsor, and as far as the authors are aware, has not been reported on in the past. The conclusions are given in Section 4.

Note that as experimental data were not available, the work reported in this paper is based on numerical predictions only. It is recommended that experimental validation be undertaken in the future. However, it is noted that conducting experiments to obtain the value of the Distortion Coefficient on the nominal wake in each case will be quite extensive and beyond the resources of the current authors. Despite the lack of experimental data to provide validation, the authors are confident that the general trends identified in this work are correct.

## 2. Materials and Methods

### 2.1. Determination of Variables

In order to model roughness, the equivalent sand roughness value,  $ks$ , was used, as discussed in [9,10]. Note that in [9], various levels of fouling were discussed in detail, ranging from a  $ks$  value of 0 (hydraulically smooth) to a  $ks$  value of 10,000, which corresponds to heavy calcareous fouling.

In this study, the value of  $ks$  was kept constant at  $ks = 2000 \mu\text{m}$ , which corresponds to the calcareous type of fouling [9]. It was assumed to be representative of the type of fouling likely in Indonesian waters.

The influence of the location and magnitude of the biofouling growth on the resistance of the submarine, and on the nominal wake, was obtained with the submarine deeply submerged.

The axis system used is shown in Figure 1, with the following abbreviations:  $AP$  = Aft Perpendicular;  $LPP$  = Length Between Perpendiculars;  $LOA$  = Length Overall;  $D$  = Hull Diameter; and  $r_{max}$  = Maximum Hull Radius.

Six different conditions for biofouling growth were investigated: All smooth, with no fouling (Case 1); all fouled (Case 2); forward one-third of length fouled only (Case 3); middle one-third of length fouled only (Case 4); stern one-third of length fouled only (Case 5); and lower portion of the hull (and aft control surfaces) fouled only (Case 6).

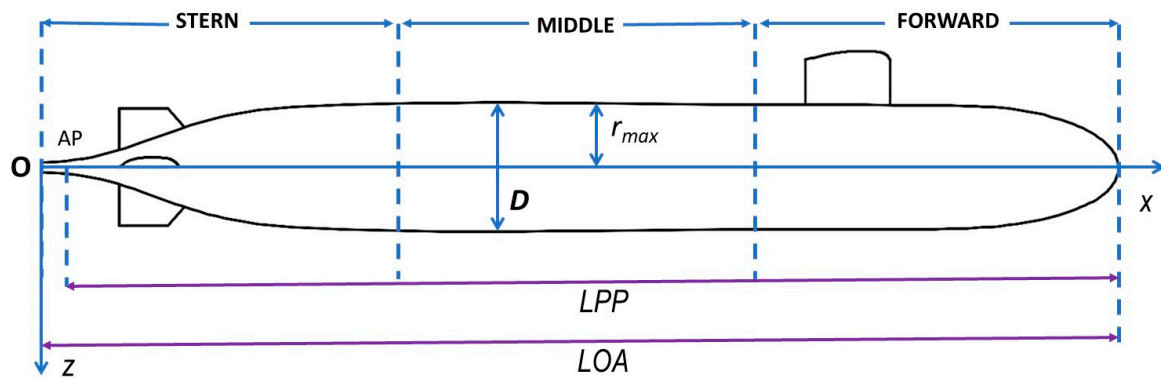


Figure 1. Schematic of hull and axis system.

This latter condition was chosen to represent the realistic situation where the upper surfaces of the boat when surfaced can be cleaned relatively easily, whereas the surfaces, which remain under the water, cannot be, as can be seen in the photograph in Figure 2. This is a photograph of a conventionally powered submarine taken by one of the authors, but similar photographs exist of nuclear-powered submarines in the public domain.



Figure 2. Example of submarine showing fouling over the lower portion of the hull.

The cases are shown schematically in Figure 3. For each case, the fouled length and fouled area are given in Table 1.

Table 1. Fouled cases.

Case	Fouled Length (m)	Fouled Wetted Surface Area (m <sup>2</sup> )
C1	-	0
C2	104.5	3676
C3	32.8	1222
C4	32.0	1229
C5	39.7	1225
C6	104.5	2025

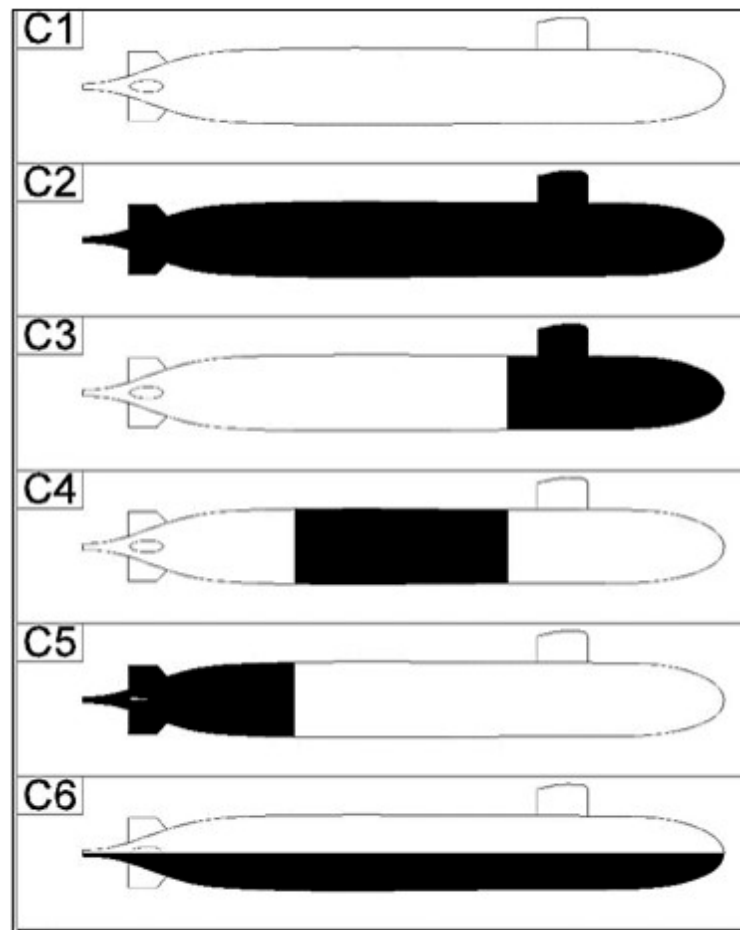


Figure 3. Variations of biofouling growth locations investigated.

Note that although the fouled length and wetted surface for Cases 3–5 are not identical, they are considered sufficiently close that the large differences in resistance are not due to these small differences in either length or wetted surface for the three cases. Due to the geometry of the submarine, it is not possible to select regions where both the length and wetted surface area are the same.

### 2.2. Numerical Simulation

Reynolds-Averaged Navier Stokes (RANS) was used to solve the governing equations in this study. RANS is the average time equation for fluid flow movement. The implementation used here is the ANSYS FLUENT commercial software as outlined in [18].

This equation is generally used to describe the turbulent flow. The equation focuses on the average flow and the effect of turbulence on the average flow property. The Reynolds-averaged equation is an equation that arises due to the interaction between variations in turbulence fluctuations and can be modeled using standard turbulent modeling techniques. The RANS equations are as follows:

Continuity:

$$\frac{\partial \bar{\rho}}{\partial t} + \text{div}(\bar{\rho} \tilde{U}) = 0 \tag{1}$$

Reynolds Equations:

$$\frac{\partial(\bar{\rho} \tilde{U})}{\partial t} + \text{div}(\bar{\rho} \tilde{U} \tilde{U}) = -\frac{\partial \bar{P}}{\partial x} + \text{div}(\mu \text{grad } \tilde{U}) + \left[ -\frac{\partial(\overline{\rho \Gamma'^2})}{\partial x} - \frac{\partial(\overline{\rho \Gamma' v'})}{\partial y} - \frac{\partial(\overline{\rho \Gamma' \underline{\Gamma}'})}{\partial z} \right] + S_{Mx}, \tag{2}$$



$$\frac{\partial(\bar{\rho}\tilde{V})}{\partial t} + \text{div}(\bar{\rho}\tilde{V}\tilde{U}) = -\frac{\partial\bar{P}}{\partial x} + \text{div}(\mu \text{grad } \tilde{V}) + \left[ -\frac{\partial(\bar{\rho}\Gamma v')}{\partial x} - \frac{\partial(\bar{\rho}v'^2)}{\partial y} - \frac{\partial(\bar{\rho}v'\underline{\omega}')}{\partial z} \right] + S_{My} \quad (3)$$

$$\frac{\partial(\bar{\rho}\tilde{W})}{\partial t} + \text{div}(\bar{\rho}\tilde{W}\tilde{U}) = -\frac{\partial\bar{P}}{\partial x} + \text{div}(\mu \text{grad } \tilde{W}) + \left[ -\frac{\partial(\bar{\rho}\Gamma'\underline{\omega}')}{\partial x} - \frac{\partial(\bar{\rho}v'\underline{\omega}')}{\partial y} - \frac{\partial(\bar{\rho}\underline{\omega}'^2)}{\partial z} \right] + S_{Mz}, \quad (4)$$

Scalar Equation:

$$\frac{\partial(\bar{\rho}\tilde{\Phi})}{\partial t} + \text{div}(\bar{\rho}\tilde{\Phi}\tilde{U}) = \text{div}(\Gamma_{\Phi} \text{grad } \tilde{\Phi}) + \left[ -\frac{\partial(\bar{\rho}\Gamma'\Phi')}{\partial x} - \frac{\partial(\bar{\rho}v'\Phi')}{\partial y} - \frac{\partial(\bar{\rho}\underline{\omega}'\Phi')}{\partial z} \right] + S_{\Phi} \quad (5)$$

Equation (1) ensures the conservation of mass in the flow such that the mass is conserved within the flow.

Equations (2)–(4) represent the conservation of momentum for three orthogonal directions in the flow. Each of these describes the acceleration mean velocity components in the respective directions. The left-hand side of these equations represents the rate of change of momentum with time.

Equation (5) is the scalar equation, which represents the conservation of the scalar quantity in the flow that governs properties such as temperature, concentration, and other scalar fields of interest.

One of the limitations of RANS models is that they are time-averaged and assume that the flow remains statistically steady. However, many practical applications involve unsteady flows, such as flows with fluctuating velocities, periodic variations, or transient phenomena. RANS models may not accurately capture unsteady behavior and may require additional methods, such as time-dependent simulations or coupling with other modeling techniques.

RANS models are widely used in engineering and scientific applications due to their computational efficiency and reasonable accuracy for many practical scenarios and are applicable to the problem being investigated here, which is about the steady-state flow around a submarine. RANS models have already been used to model roughness effects, as discussed in [19,20], where the validity of using such models to investigate the effect of roughness on ship resistance was demonstrated. The work in this paper adopted the same approach, where a roughness function is applied, and the wall functions are modified as given in Equation (6).

$$U^+ = \frac{1}{\kappa} \ln y^+ + B - \Delta U^+ \quad (6)$$

In Equation (6),  $U^+$  is the non-dimensional velocity in the boundary layer,  $\kappa$  is the von Karman constant equal to 0.42,  $y^+$  is the non-dimensional normal distance to the wall,  $B$  is the smooth wall log-law intercept, and  $\Delta U^+$  is the roughness function.

For the present work, the  $k-\epsilon$  turbulence model was selected, as this is commonly used in this field, and is generally considered acceptable. To handle different boundary layer thicknesses in the flow fields (such as the hull of the submarine and its appendages), the whole  $y^+$  formulation was employed, enabling automatic switching between low and high Reynolds boundary wall models. The numerical solver used for the simulations is based on the finite volume method, which discretizes the RANS equations. In this approach, a segregated model was utilized in the solver, and the convection terms were discretized using the second-order upwind scheme to enhance solution accuracy. The criterion for the near wall is between 30 and 100, and the value of  $y^+$  for the present case is 84.

### 2.3. DARPA Suboff Submarine Geometry and Boundary Conditions

The submarine model that was simulated in this study is the DARPA Suboff model submarine [21]. Its principal particulars are given in Table 2. The biofouling condition was used in a previous study and represents typical conditions for biofouling in Indonesian waters.

**Table 2.** Comparison of actual values with modelled values.

Parameter	Actual	Model	Units
Length Overall ( <i>LOA</i> )	104.5	104.5	m
Length Between Perpendiculars ( <i>LPP</i> )	104.5	102.3	m
Hull Diameter ( <i>D</i> )	12.2	12.2	m
Wetted Surface ( <i>S</i> )	3656.4	3689.7	m <sup>2</sup>
Volume ( $\nabla$ )	9759.7	9730.2	m <sup>3</sup>

The DARPA Suboff submarine was modelled using Maxsurf software [22]. The principal parameters obtained from the Maxsurf modeler are compared with the actual DARPA Suboff model data in Table 2. As can be seen, the difference in the wetted surface area and the volume are sufficiently small to be considered negligible.

The domain for this analysis was chosen to simulate the flow around the submarine hull at full scale. The domain is defined with a rectangle length of  $5LPP$  as shown in Figure 4. The bow was used as the reference point with twice the  $LPP$  in the forward direction and three times the  $LPP$  in the aft direction. This dimension is recommended by the ITTC [23].

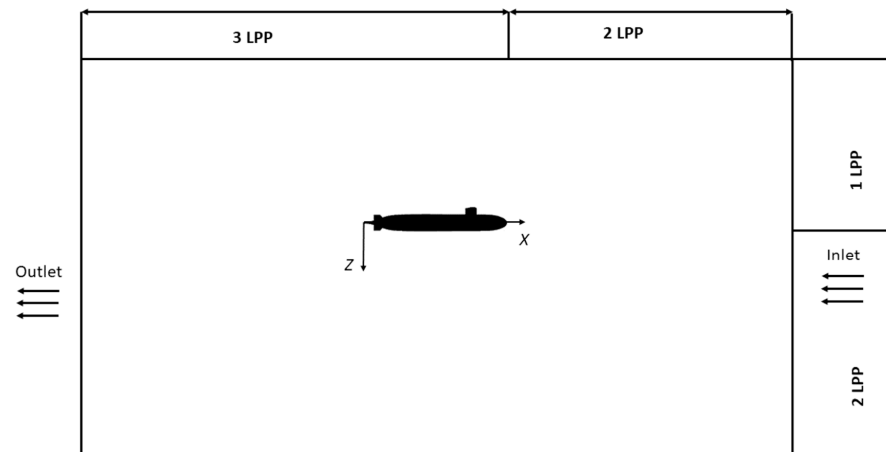


**Figure 4.** Computational domain.

Initially, the boundary conditions were determined by selecting areas defined as flow inputs and outputs. The appropriate boundary conditions were selected to ensure the accuracy of the numerical modeling of the computation.

As can be seen in Figure 4, the domain is slightly asymmetric with a smaller distance from the submarine to the top of the domain compared to the distance between the submarine and the bottom of the domain. This is because earlier work conducted by the authors made use of the free surface. However, for this work, the influence of the free surface is considered negligible.

The input speed at the inlet was 9.14 m/s throughout this work, giving a Reynolds number of  $1 \times 10^9$ . The submarine hull was assumed to be a wall with no-slip conditions, fitting the kinematic boundary conditions.

### 2.4. Mesh Generation

Adaptation to determine the elements in the grid structure is very influential and is one of the challenges in most hydrodynamic simulations. Any errors can be minimized

by determining the mesh size and type to complete the computation. The analysis in this paper uses the RANS equations. A triangular mesh is used over the entire area to reduce the number of computations in the computational domain.

There are two meshing techniques used, namely the body of influence technique, and element sizing. The body of influence technique is where the element size is affected by the location, such that elements that are far from the body have relatively larger sizes than those that are near the body. This was used to focus on the volume of most interest and is a very suitable technique for viewing wakes that occur around the surface of the submarine, and into the propeller.

Mesh independence is carried out by using uncertainty determination from the numerical studies and adequate grid spacing, determining stable mesh dimensions for the simulation. The technique used is the Grid Independence Study, which is recommended by the ITTC [23] to ensure correct computation. This method is widely used and was initially proposed by Roache [24]. The determination of the refinement mesh in the body of influence area captures turbulence that occurs on the surface of the submarine hull due to biofouling. This is the same as applying a smooth mesh to the surface of the submarine hull, which has been proven to increase accuracy and has been tested by Duan et al. [25] with a focus on the net components around the hull area.

The grid independence study was carried out at a speed of 9.14 m/s in Case 1. The influence of the body technique was used to design the different grid sizes.

The parameter used was the total resistance. There are six simulations from small to large element determination in the range of 0 to 3,500,000 total elements. When the difference obtained with the different grid sizes is not more than 2%, the result is considered to be sufficiently independent of grid size, and hence the size of the grid required can be obtained.

The results of the Grid Independence Study can be seen in Figure 5. From this figure, it can be seen that the deviation of the total number of elements between 1.947 and 3.495 million is below 2% for all parameters. This means that the grid independence values are met because they do not exceed 2%. Therefore, a computation with a total of 1.947 million elements was used for the simulations presented here.

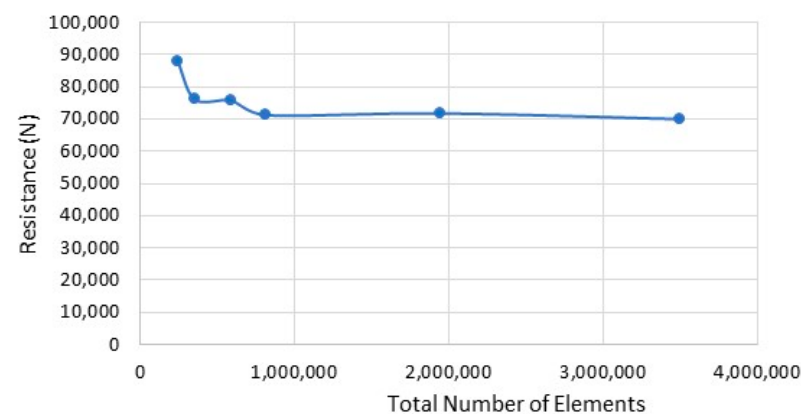


**Figure 5.** Results of grid independence study.

The roughness due to biofouling was not modelled directly but rather included in the boundary conditions using a wall function.

### 3. Results

#### 3.1. Effect of Biofouling on Submarine Resistance

The total resistance coefficient ( $C_T$ ) of a fully submerged submarine is made up of the viscous pressure resistance coefficient ( $C_P$ ) and the friction resistance coefficient ( $C_F$ ), as shown in Equation (7). Note that the friction resistance coefficient on the submarine will be slightly greater than the flat plate resistance coefficient often quoted [11]. It is important



to recognize that there will not be any wave-making resistance when the submarine is deeply submerged.

$$C_T = C_P + C_F \tag{7}$$

The total resistance coefficient ( $C_T$ ), as defined by Equation (8), and the friction resistance coefficient, as defined by Equation (9), are given for the six cases in Table 3.

$$C_T = \frac{\text{Total resistance}}{\frac{1}{2}\rho V^2 S} \tag{8}$$

$$C_F = \frac{\text{Friction resistance}}{\frac{1}{2}\rho V^2 S} \tag{9}$$

**Table 3.** Non-dimensional resistance coefficient at  $V = 9.14$  m/s for each case.

Case	$C_T (\times 10^{-3})$	$C_F (\times 10^{-3})$	Increase in $C_F$ (Compared to C1)	% Increase (Compared to C1)
C1	1.93	1.61	-	-
C2	3.52	3.20	1.59	99
C3	2.42	2.10	0.49	30
C4	2.28	1.96	0.35	22
C5	2.24	1.92	0.31	19
C6	2.85	2.53	0.92	57

The condition of the hull that has the greatest resistance is Case 2, where the hull is completely covered with biofouling. This increase is due to the increase in friction resistance. The increase in the friction resistance coefficient between the smooth submarine (Case 1) and the fully fouled case (Case 2) is approximately 99%, representing almost double the friction resistance coefficient when fouled. As this is such a large component of the total resistance coefficient, the increase in the total resistance coefficient is approximately 82%.

When the hull is only partially covered by fouling, the longitudinal location of biofouling growth that causes the greatest increase in friction resistance coefficient is the bow section (Case 3). The increase in the friction resistance coefficient between the smooth submarine and the one with only the forward one-third of the bow covered in biofouling (Case 3) is approximately 30%.

The fouling over only the mid-length of the hull, or over only the aft third of the hull, results in a lower increase in the friction resistance coefficient than fouling over only the forward third of the hull (22% and 19%, respectively). Although there are very slight differences in the fouled area and fouled length for each of these cases (see Table 1), each of these cases corresponds to approximately 33% of the hull area being fouled. Thus, the differences in the increase in frictional resistance coefficient are due to the longitudinal location of the fouled area, not to the size of the fouled area. This finding corresponds to the results of other work, such as [10,15].

Of particular interest is the case where the lower half only of the submarine is fouled (Case 6). This represents the situation where cleaning has occurred on the exposed parts when the submarine is on the surface (Figure 2). Here it is assumed that the upper half of the submarine can be reached for cleaning; however, the lower half cannot. Or it may be that in a foreign port cleaning of the lower part of the hull is prohibited in order to reduce the transmission of invasive species [17]. This is a realistic scenario, as demonstrated by Figure 2, and numerous other photographs of submarines on the surface.

In this case, the increase in the friction resistance coefficient compared to the fully clean hull is approximately 57%. Importantly, the friction resistance coefficient of the hull with the lower half fouled is approximately 20% less than the fully fouled case. The fouled

area of the lower half of the submarine (Case 6) is approximately 45% of the total area of the submarine. This implies that even if it is only possible to keep the upper portion of the submarine free of fouling, this is worth doing.

### 3.2. Effect of Biofouling on Turbulence

Figure 6 shows the level of turbulence over the top and bottom of the hull in all six cases. As expected, the clean case, Case 1, shows the least turbulence, whereas the fully fouled case, Case 2, shows the most turbulence. Of particular interest is the level of turbulence over the stern of the hull, which is much higher when the hull is fouled, compared to when it is clean.

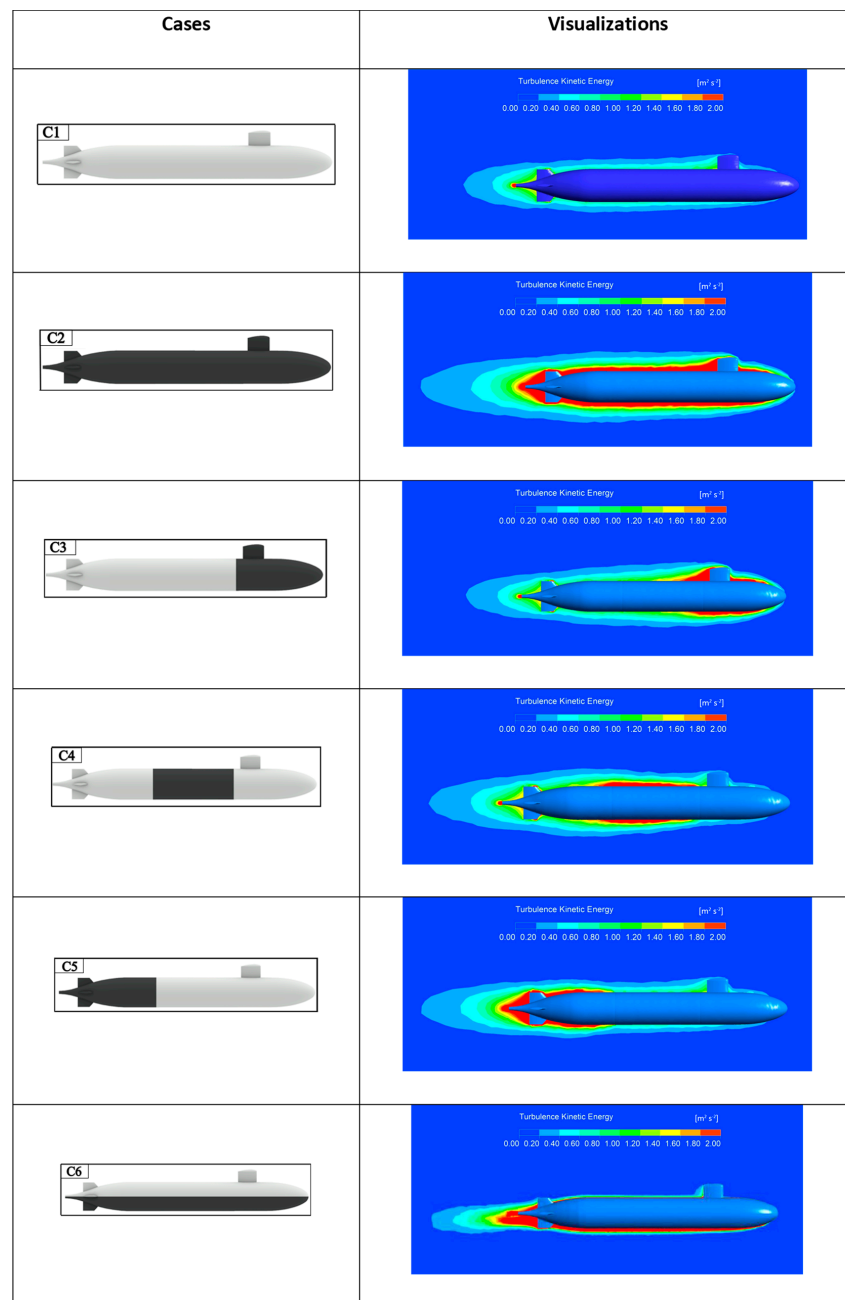


Figure 6. Visualization of turbulent flow at a speed of 9.14 m/s.

When the fouling is only on the forward one-third of the hull, Case 3, considerable turbulence can be seen corresponding to the fouled region; however, the level of turbulence diminishes aft of this and is almost the same as the fully clean case at the stern.

Conversely, when the fouling is only over the aft one-third of the hull, Case 5, the turbulence level ahead of the fouled region is low, similar to the clean case, Case 1, but the turbulence level is then very high over the stern of the hull, similar to the fully fouled case, Case 2. This implies that the nominal wake at the location of the propeller for the case where there is only fouling over the aft one-third of the hull is similar to that when the whole of the submarine hull is fouled.

As expected, when the fouling is only on the lower half of the hull, the turbulence level over the bottom of the hull is similar to the turbulence level over the bottom of the hull for the fully fouled case, Case 2, and the turbulence level over the top of the hull is similar to that in the clean case, Case 1. In this case, the lower part of the hull at the stern has a high degree of turbulence, whereas the upper part of the hull at the stern has a low degree of turbulence. This will clearly affect the nominal wake, and in particular, could influence the circumferential wake distribution.

### 3.3. Effect of Biofouling on Wake

The wake flow into a submarine’s propulsor has a major influence on its unsteady loading, and hence the noise it generates, as discussed in [11]. For Suboff, the propeller is located 1m ahead of the Aft Perpendicular (AP).

The nominal wake distribution at the propeller plane for the submarine at a speed of 9.14 m/s is shown for the six cases tested in Figure 7. The magnitude of the axial velocity is indicated by the different colors, where the scales are the same for each case.

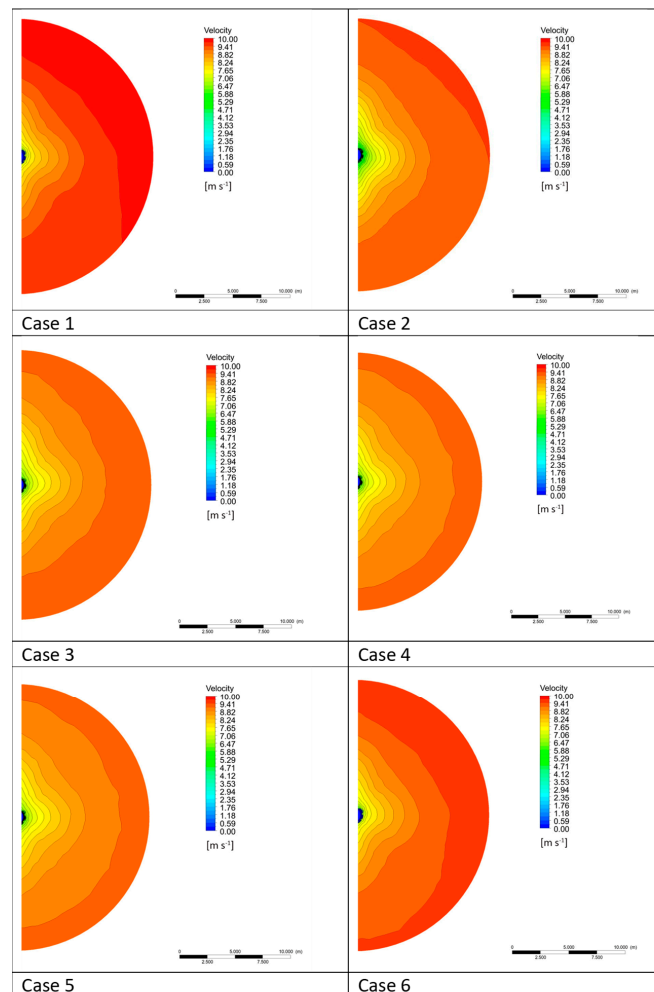


**Figure 7.** Nominal wake at propeller location for all six cases (1m forward of the AP). Note that the domain shown extends to twice the maximum hull diameter.

The variation of the wake in a circumferential sense can lead to increased noise on the propeller due to the changing blade load as the propeller rotates around the circumference. Where the wake is greater, and hence the axial flow ( $V^*$ ) is smaller, the angle of attack of the flow into the propeller is higher than when the wake is lower, as illustrated in Figure 8.

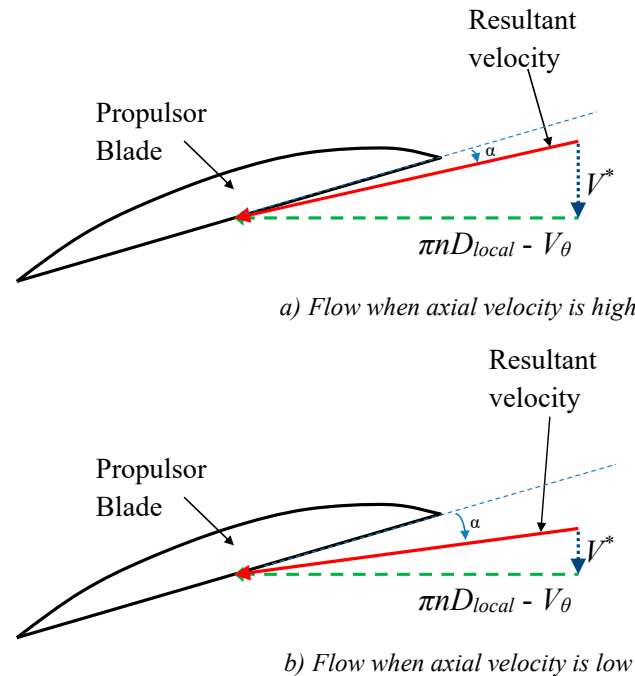


Figure 8. Influence of axial flow velocity on flow into propeller blade at  $D_{local}$ .

In Figure 8,  $n$  is the rotational speed of the propeller in revolutions per second,  $D_{local}$  is the local diameter being considered,  $V^*$  is the local axial flow into the propeller blade, and  $V_{\theta}$  is the local tangential velocity into the propeller blade and the angle of attack of the blade is  $\alpha$ .

Although Figure 7 shows the distribution of the axial wake at the propeller plane for each case, it is difficult to assess the magnitude of the unsteadiness of the wake in a circumferential sense, and hence difficult to make a quantitative assessment of this from that figure.

One way of assessing the magnitude of the unsteadiness of the wake in a circumferential direction is by using the Distortion Coefficient ( $DC$ ) as developed by Seil and Anderson [16] and explained in [11]. The Distortion Coefficient is given by Equation (10) and is calculated for a given radius.

$$DC = \sqrt{\frac{\sum_{i=1}^n (w_i - \bar{w})^2}{n - 1}} \tag{10}$$

In Equation (10),  $w_i$  is the wake at point “ $i$ ” on the radius, where there are  $n$  such points, and  $\bar{w}$  is the average wake at that radius. The calculation can be carried out for each radius from the hub as far outwards as desired. The value of  $DC$  can then be plotted as a function of the radius, and this gives a quantitative measure of the level of circumferential unsteadiness of the wake—the factor influencing the dynamic unsteady loading on the propulsor. This can be used in a qualitative manner to assess the influence that various wakes will have on the noise that the propulsor will generate. To the authors’ knowledge, such information has not been reported before and is of significant importance to the operation of submarines, as it will influence the noise generated by the propeller.

Figure 9 shows the value of  $DC$  for each of the six cases as functions of  $r/r_{max}$  where  $r_{max}$  is the hull radius and  $r$  is the radius of the circumference analyzed. A submarine

propeller will typically have a radius less than  $r_{max}$  and hence the area of interest is likely to be for  $r/r_{max}$  values less than one.

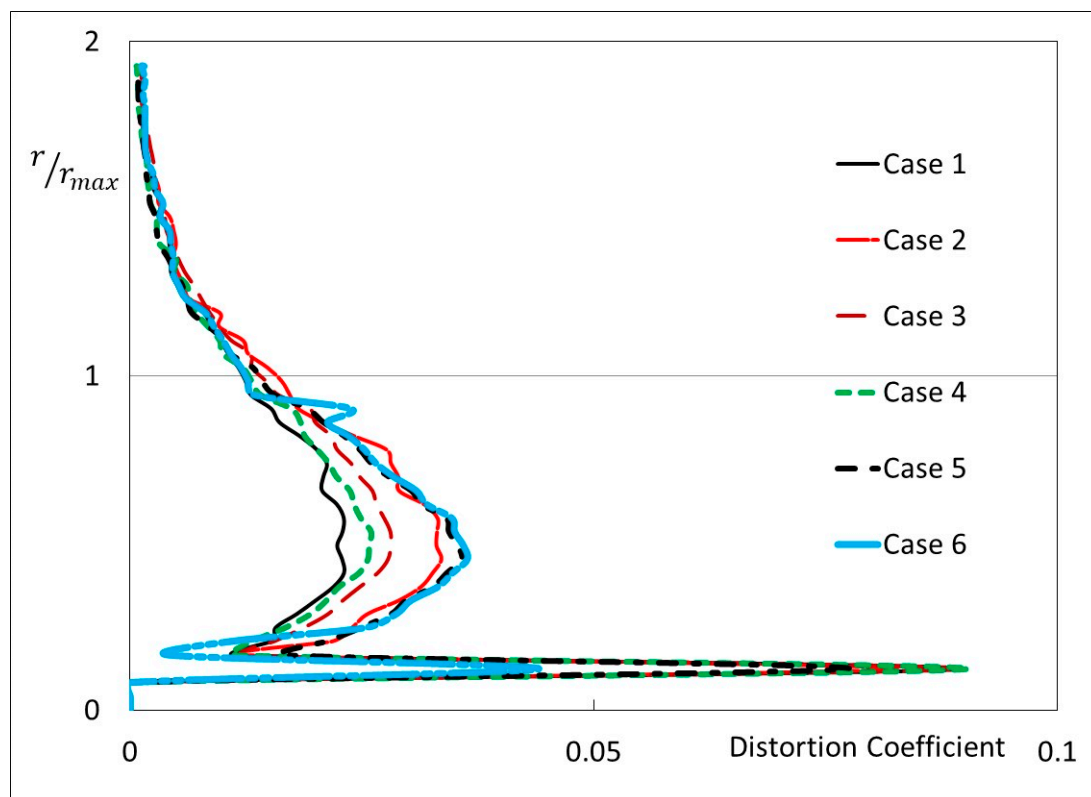


Figure 9. Distortion coefficient.

As can be seen from Figure 9, when there is no fouling (Case 1), the Distortion Coefficient has the lowest value for most of the radius compared to the other five cases. When the whole of the submarine is fouled (Case 2), the Distortion Coefficient is much higher, indicating that the propulsor is likely to generate more noise in this case. Case 5, with only the aft one-third of the submarine fouled, has similar values of the Distortion Coefficient to Case 2, the fully fouled case, whereas the results for Cases 3 and 4 are much closer to the clean case. This appears to show that there is an improvement in the wake along the hull aft of the fouled region.

Case 6, with the lower half of the submarine fouled along its whole length, has values of the Distortion Coefficient close to those of the fully fouled case, other than for very small values of  $r/r_{max}$ . The reason for the lower values of the Distortion Coefficient for the smaller values of  $r/r_{max}$  is not clear and requires further investigation.

#### 4. Conclusions

Biofouling increases the resistance coefficient of a submarine compared to a clean hull. When biofouling is only located on the forward one-third of the hull, the increase in the resistance coefficient is still substantial. However, if biofouling is only located further aft on the hull, then the increase in the resistance coefficient is not as large.

When biofouling is located on the whole length of the lower half of the submarine, the increase in the resistance coefficient compared to a smooth hull is approximately half that when the whole submarine is fouled. This indicates that cleaning the upper half of the submarine, when possible, is advantageous.

The level of turbulence is influenced by the fouling. The clean case shows the least turbulence, whereas the fully fouled case shows the most turbulence. The level of turbulence over the stern of the hull is much higher when the hull is fouled, compared to when it is clean. When the fouling is on only the forward one-third of the hull, considerable



turbulence can be seen corresponding to the fouled region. However, the level of turbulence diminishes aft of this and is almost the same as the fully clean case at the stern.

Conversely, when the fouling is over only the aft one-third of the hull, the turbulence level ahead of the fouled region is low, similar to the clean case. However, the turbulence level is then very high over the stern of the hull, similar to the fully fouled case. This implies that fouling over the stern region will influence the nominal wake to a greater extent than fouling over the forward region of the hull.

When the fouling is only on the lower half of the hull, the turbulence level over the bottom of the hull is similar to the turbulence level over the bottom of the hull for the fully fouled case and the turbulence level over the top of the hull is similar to that in the clean case. In this case, the lower part of the hull at the stern has a high degree of turbulence, whereas the upper part of the hull at the stern has a low degree of turbulence. This will clearly affect the nominal wake, and in particular, could influence the circumferential wake distribution. As it is likely that a greater circumferential variation in wake will increase the noise that the propeller makes, this is of great importance to a submarine.

Biofouling over the whole hull results in an increase in the circumferential variation of the nominal wake at the propeller plane, as assessed by the Distortion Coefficient (DC). However, if biofouling is only located forward on the hull, the increase in the value of DC is much less than if it is only located aft. This is of significant importance to the operation of the submarine as it directly influences the noise generated by the propulsor and has not been shown before.

When biofouling is only located along the whole length of the lower half of the hull, the value of DC is close to that when the whole of the submarine is covered by biofouling, other than for very small values of  $r/r_{max}$ . The reason for this is unclear.

It is recommended that experiments be undertaken to measure the nominal wake for the cases covered in this paper, in order to validate the results presented here.

**Author Contributions:** Conceptualization, R.C.A., A.N., F.F., I.K.A.P.U. and M.R.R.; methodology, R.C.A., I.K.A.P.U. and M.R.R.; software, R.C.A.; validation, R.C.A.; formal analysis, R.C.A.; investigation, R.C.A., I.K.A.P.U. and M.R.R.; resources, I.K.A.P.U.; data curation, R.C.A.; writing—original draft preparation, R.C.A., I.K.A.P.U. and M.R.R.; writing—review and editing, R.C.A., A.N., I.K.A.P.U. and M.R.R.; visualization, R.C.A.; supervision, I.K.A.P.U. and M.R.R.; project administration, I.K.A.P.U.; funding acquisition, I.K.A.P.U. All authors have read and agreed to the published version of the manuscript.

**Funding:** The research described in this paper was partly funded by the World Class Professor (WCP-Like) Program Batch 2 from the Institut Teknologi Sepuluh Nopember (ITS) with award number: 1855/IT2/T/HK.00.01/2022.

**Institutional Review Board Statement:** Not applicable.

**Informed Consent Statement:** Not applicable.

**Data Availability Statement:** Not applicable.

**Acknowledgments:** Sutiyo of the Hang Tuah University, Surabaya, assisted with the CFD work and the authors are grateful for his help.

**Conflicts of Interest:** The authors declare no conflict of interest.

## References

1. Woods Hole Oceanographic Institution [WHOI]. *Marine Fouling and Its Prevention*; Contribution No 580; United States Naval Institute: Annapolis, MD, USA, 1952.
2. Townsin, R.L.; Byrne, D.; Sevensen, T.E.; Milne, A. Estimating the technical and economic penalties of hull and propeller roughness. *Trans. SNAME* **1981**, *89*, 295–318.
3. Townsin, R.L. The ship hull fouling penalty. *Biofouling* **2003**, *19*, 9–16. [[CrossRef](#)] [[PubMed](#)]
4. Naval Ships' Technical Manual [NSTM]. *Waterborne Underwater Hull Cleaning of Navy Ships*; S9086-CQ-STM-010; Naval Sea Systems Command: Washington, DC, USA, 2006; Chapter 081.

5. Schultz, M.P.; Bendick, J.A.; Holm, E.R.; Hertel, W.M. Economic Impact of Biofouling on a Naval Surface Ship. *J. Bioadhesion Biofilm. Res.* **2020**, *27*, 87–98. [[CrossRef](#)] [[PubMed](#)]
6. Arndt, E.; Robinson, A.; Hester, S. *Factors That Influence Vessel Biofouling and Its Prevention and Management*; Final Report for CEBRA Project 190803; Center of Excellence for Biosecurity Risk Analysis: Melbourne, Australia, 2021.
7. Hadzic, N.; Gatin, I.; Uroic, T.; Lozar, V. Biofouling dynamic and its impact on ship powering and dry-docking. *Ocean. Eng.* **2022**, *245*, 110522. [[CrossRef](#)]
8. Bakka, H.; Rognebakke, H.; Glad, I.; Hobaek, I.; Vanem, H. Estimating the effect of biofouling on ship shaft power based on sensor measurements. *Ship Technol. Res.* **2020**. [[CrossRef](#)]
9. Uzun, D.; Demirel, Y.K.; Coraddu, A.; Turan, O. Time-Dependent biofouling growth model for predicting the effects of biofouling on ship resistance and powering. *Ocean. Eng.* **2019**, *191*, 106432. [[CrossRef](#)]
10. Uzun, D.; Ozyurt, R.R.; Demirel, Y.K.; Turan, O. Does the barnacle settlement pattern affect ship resistance and powering. *Appl. Ocean. Res.* **2020**, *95*, 102020. [[CrossRef](#)]
11. Renilson, M.R. *Submarine Hydrodynamics*, 2nd ed.; Springer: Berlin/Heidelberg, Germany, 2018; ISBN 978-3-319-79056-5.
12. Uzun, D.; Sezen, S.; Ozyurt, R.; Atlar, M.; Turan, O. A CFD study: Influence of biofouling on a full-scale submarine. *Appl. Ocean. Res.* **2021**, *109*, 102561. [[CrossRef](#)]
13. Uzun, D.; Sezen, S.; Atlar, M.; Turan, O. Effect of biofouling roughness on the full-scale powering performance of a submarine. *Ocean. Eng.* **2021**, *238*, 109773. [[CrossRef](#)]
14. Song, S.; Terziev, M.; Tezdogan, T.; Demirel, Y.K.; Muscat-Fenech, C.D.M.; Incecik, A. Investigating roughness effects on ship resistance in shallow waters. *Ocean. Eng.* **2023**, *270*, 113643. [[CrossRef](#)]
15. Suastika, I.K.; Hakim, M.L.; Nugroho, B.; Nasirudin, A.; Utama, I.K.A.P.; Monty, J.P.; Ganapathisubramani, B. Characteristics of drag due to streamwise inhomogeneous roughness. *Ocean. Eng.* **2021**, *223*, 108632. [[CrossRef](#)]
16. Seil, G.J.; Anderson, B. A comparison of submarine fin geometry on the performance of a generic submarine. In Proceedings of the Pacific 2012, International Maritime Conference, Sydney, Australia, 30 January–2 February 2012.
17. Raiston, E.; Swain, G. The Effect of Husbandry and Original Location on the Fouling of Transplanted Panels. *J. Mar. Sci. Eng.* **2023**, *11*, 478. [[CrossRef](#)]
18. ANSYS for Researchers. *User's Guide*; ANSYS Inc.: Burlington, MA, USA, 2022.
19. Song, S.; Demirel, Y.K.; Atlar, M.; Dai, S.; Day, S.; Turan, O. Validation of the CFD approach for modelling roughness effect on ship resistance. In Proceedings of the Sixth International Conference on Advanced Model Measurement Technology for the Maritime Industry, Rome, Italy, 9–11 October 2019.
20. Mikkelsen, H.; Walther, J.H. Effect of roughness in full-scale validation of a CFD model of self-propelled ships. *Appl. Ocean. Res.* **2020**, *99*, 102162. [[CrossRef](#)]
21. Groves, N.C.; Huang, T.T.; Chang, M.S. *Geometric Characteristics of DARPA Suboff Models (DTRC Model Nos 5470 and 5471)*; David Taylor Research Center: Bethesda, MD, USA, 1989.
22. Bentley. *Bentley Modeller Program and User Manual, Maxsurf Modeller CONNECT*, 23rd ed.; Bentley Systems Incorporated: Exton, PA, USA, 2022.
23. ITTC. Practical Guidelines for Ship CFD Applications. ITTC-Recommended Procedures and Guidelines; 2014. Available online: [https://itc.info/media/9876/0\\_0.pdf](https://itc.info/media/9876/0_0.pdf) (accessed on 6 May 2023).
24. Roach, P. Verification of Codes and Calculations. *AIAA J.* **1998**, *36*, 5.
25. Duan, X.; Sun, W.; Chen, C.; Wei, M.; Yang, Y. Numerical investigation of the propoising motion of a seaplane planing on water with high speeds. *Aerosp. Sci. Technol.* **2019**, *84*, 980–994. [[CrossRef](#)]

**Disclaimer/Publisher's Note:** The statements, opinions and data contained in all publications are solely those of the individual author(s) and contributor(s) and not of MDPI and/or the editor(s). MDPI and/or the editor(s) disclaim responsibility for any injury to people or property resulting from any ideas, methods, instructions or products referred to in the content.